Variability of an early developmental cell population underlies stochastic laterality defects

Roberto Moreno-Ayala[1], Pedro Olivares-Chauvet[1], Ronny Schäfer[1], Jan Philipp Junker[1,*]

[1] Max Delbrück Center for Molecular Medicine, Berlin Institute for Medical Systems Biology

[*] Correspondence: janphilipp.junker@mdc-berlin.de

Summary

Embryonic development seemingly proceeds with almost perfect precision. However, it is largely unknown how much microscopic variability is hidden beneath this macroscopic accuracy. Here, we quantified embryo-to-embryo variability in vertebrate development, by studying cell number variation in the zebrafish endoderm. We noticed that the size of a sub-population of the endoderm, the dorsal forerunner cells (which later form the left-right organizer), is highly variable between individual embryos. We found that the frequency of left-right laterality defects is increased drastically in embryos with a low number of dorsal forerunner cells, and we observed that these fluctuations are largely nonhereditary. Hence, a stochastic variation in early development leads to a remarkably strong macroscopic phenotype. These fluctuations appear to be caused by variable deposition of maternal factors involved in specification of the dorsal forerunner cells. In summary, we here dissect cause and consequence of embryo-to-embryo variability in a vertebrate model.

Introduction

During embryogenesis, cells acquire their identity due to a combination of external signaling cues and internal competence factors. Embryonic development is remarkably robust towards fluctuations of regulatory factors such as morphogen levels (Barkai and Shilo 2009; Briscoe and Small 2015) or genetic variation (El-Brolosy et al. 2019). However, developmental

buffering of fluctuations is not perfect, and phenotypic variation can even be observed in mutants from isogenic *C. elegans* strains raised under identical environmental conditions due to noisy gene expression and stochastic variation in genetic interaction partners (Burga, Casanueva, and Lehner 2011; A. Raj et al. 2010).

Differences in the size of progenitor populations may be another important source of phenotypic variability in higher organisms. However, the degree of variability in cellular ontogenies and their potential phenotypic consequences remain largely unknown. Some notable exceptions are: changes in the subdivision of the primordium that gives rise to the head sensory organs lead to fluctuations in ommatidia number at different levels (inter-individual, inter-strain and inter-specific) in the *Drosophila* genus (Ramaekers et al. 2019; Gaspar et al. 2020); sexual dimorphism and left-right asymmetry of ommatidia number in the ant *Temnothorax albipennis* are related to differences in mating and motion behavior, respectively (Hunt et al. 2018). Here, we set out to systematically quantify the degree of inter-individual cell number variation and its phenotypic consequences, using endoderm specification in the early zebrafish embryo as a model system.

The endoderm, which is induced by high levels of Nodal signaling during early development, contributes to the formation of liver, pancreas, intestine, stomach, pharynx and swim bladder (Warga and Nüsslein-Volhard 1999). The dorsal forerunner cells (DFCs) are a small group of cells, considered a subset of the endoderm (Alexander et al. 1999; Warga and Kane 2018) (Figure 1A). They are the precursors of the Kupffer's vesicle (KV) (Melby, Warga, and Kimmel 1996), the organ that determines left-right asymmetry in the embryo (Essner et al. 2005) (Figure 1B). Since the endoderm is the smallest germ layer during early zebrafish development (Shah et al. 2019) and the DFCs comprise only a few dozen cells (Oteíza et al. 2008; Gokey, Dasgupta, and Amack 2015), we asked if naturally occurring embryo-to-embryo variation in cell numbers in wild-type embryos could have any phenotypic consequences.

Results

To characterize cell number variability during zebrafish early embryogenesis, we counted the number of endodermal cells and DFCs at the 75% epiboly stage using a Tg[*sox17*:GFP] reporter line (Figure S1A-D). We found that the number of endodermal cells exhibits considerable variation, with ~500-800 cells per embryo (Figure 1C). However, the number of DFCs is even more variable, ranging from ~10 to ~50 cells per embryo (Figure 1D). This variation of DFC numbers persists at a later stage when they have formed the KV (Figure 1E, Figure S1E), suggesting that no corrective mechanisms are triggered in the animals with particularly high or low numbers of DFCs. We did not find a positive correlation between total cell number and either the endoderm or the DFCs population (Figure 1C, D), indicating that this variation is not due to staging differences. Furthermore, we found no association between the number of DFCs and the number of endodermal cells (Figure S1F), which suggests that the fluctuations of these two cell populations have independent sources.

The surprisingly large fluctuations in DFC numbers prompted us to investigate possible phenotypic consequences of this variation at later developmental stages. Since the DFCs give rise to the KV, the organ establishing left-right asymmetry, we focused on investigating possible laterality defects. Previous experimental studies, as well as mathematical modeling, suggested that the size of the KV needs to exceed a certain threshold in order to enable reliable left-right patterning (Sampaio et al. 2014; Gokey et al. 2015). As the heart is the first organ that is formed during zebrafish development, and since its laterality can be assessed easily in live embryos, we examined the percentage of embryos with defective heart laterality (DHL) in different clutches of embryos (Tüpfel long-fin (TL) wildtype strain) at prim-22 stage (Figure 2A; Video 1). We found a DHL average of 3.9% [standard deviation (sd): 3.0%, 53 independent observations (IO), total amount of scored embryos (n): 6081]. Even though this is a remarkably high frequency for a wildtype population, this value is in very good agreement with previous

reports based on *in situ* hybridization of lower sample numbers (Wang et al. 2011: 3%, n = 650; Noël et al. 2013: 6%, n = 387).

We then evaluated whether a change in the environmental conditions could unmask an underlying sensitivity in individuals that would otherwise present normal organ laterality. Previous reports have observed an influence of temperature on the penetrance of zebrafish mutant phenotypes (Imai et al. 2001). The incubation temperature for zebrafish embryos ranges from 25°C to 33°C, with 28.5ºC being the (Kimmel et al. 1995). Increasing the temperature to 33ºC led to a remarkable increase of the DHL average to 26.4% (sd = 9%, IO = 89, n = 9557) (Figure 2A). We observed no difference in the mortality rate, and the fraction of abnormal embryos (which were excluded from analysis in any condition) remained moderate (4.6% and 12.1% of the embryos showed a swollen heart cavity or tail defects at 28.5°C and 33°C, respectively). Taken together, these observations suggest that establishment of left-right laterality in zebrafish is relatively unstable, which we hypothesized might be due to the variable number of DFCs.

To test this idea, we set out to determine whether the measured fluctuations in DFC numbers are directly linked to the observed laterality variation. To do so, we counted the number of DFCs by live microscopy at 60% epiboly stage and assessed the laterality of the heart and the liver at later stages, after incubation at 33ºC. We found that the number of DFCs at 60% epiboly is strongly predictive of laterality defects by long pec stage (Figure 2B), which establishes a direct association between DFC numbers and laterality defects. Of note, we observed that the fraction of embryos with laterality defects is ~50% for those individuals with less than ~20 DFCs, suggesting that laterality is established randomly (and hence half of the time correctly) in embryos with low DFC number. In summary, we found that an early fluctuation of the size of a small cell population is correlated with a macroscopic defect at later stages, rather than be being corrected over the course of development.

We then aimed to exploit the influence of temperature as a tool to better understand the mechanism of how variability in DFC numbers influences the frequency of heart laterality defects. To this end, we tested several temperature shift treatments spanning early development (1-cell to bud stage), early somitogenesis (bud to 14-somites stage) and organogenesis (following 14-somite stage) (Figure 2C). Interestingly, we found that treating the embryos during early somitogenesis alone, the time at which the KV is formed, was sufficient to generate a similar DHL frequency as with continuous incubation at 33°C (Figure 2C, III). This result suggests that the temperature treatment mostly influences KV function (and hence global left-right patterning). However, temperature does not have a major influence on specification of DFCs, which happens before somitogenesis, or heart looping, which happens after somitogenesis. To corroborate this hypothesis, we decided to investigate potential defects of global left-right patterning mediated by the KV. Rotational movements by cilia create a directional fluid flow in the extracellular space that triggers the activation of Nodal signaling on the left lateral plate mesoderm by inducing degradation of the Nodal antagonist *dand5* on the left side. This leads to expression of the Nodal ligand *southpaw* (*spaw*) only on the left side of the lateral plate mesoderm (Hashimoto et al. 2004), which is the molecular signal used to establish organ laterality. Indeed, we found that asymmetric expression of *dand5* was reduced at 33ºC compared to 28.5ºC (Figure S2A,B), suggesting that the elevated temperature interferes with the patterning activity of the KV.

To gain further insight into how the number of cells is related to the function of the KV, we measured the size of the KV as well as the number of cells (Figure S2C-E). We found that, as expected, the size of the KV and the number of cells are correlated (R^2 = 0.78 for 28.5ºC, 0.58 for 33ºC). However, while the number of cells remained similar, the size of the KV lumen was significantly decreased at 33ºC compared to 28.5ºC. Taken together, these results suggest that an elevated temperature leads to a lowering of the cell threshold required for reliable

functioning of the KV, which is mediated at least partially via a reduction of the size of the lumen.

In line with these observations, we found a gradient of expression patterns for the early left-right marker gene *spaw*, ranging from the expected pattern (i.e. *spaw* only on the left) to bilateral expression (*spaw* visible on both sides, although not necessarily at the same level) and complete reversal (i.e. *spaw* only on the right) (Figure 2D). We hypothesized that these defects on the level of *spaw* expression should produce concordant laterality defects in different organs that exhibit left-right asymmetry, such as the heart and liver. Indeed, we found that in most, but not all, cases the embryos with reversed heart laterality also exhibited reversed liver laterality (Figure 2E). We speculate that discordant organ laterality might occur in case of almost perfectly balanced bilateral *spaw* expression (i.e., the same expression levels on both sides), leading to a scenario where in some cases the two organs would develop their laterality largely randomly and independently from each other.

After observing this strong and macroscopically visible phenotype caused by cell number fluctuations at very early developmental stages, we wanted to understand the origin of the DFC number fluctuations. First, we set out to distinguish stochastic fluctuations from genetically determined variation of cell numbers. To identify possible genetic factors, we raised embryos with a reversed heart loop to adulthood and evaluated the DHL frequency on their progeny. As a control, embryos with normal heart laterality were raised as well. To our surprise, we detected no significant differences in the percentage of reversed heart laterality in the offspring compared to the control group, at either 28.5°C or 33°C (Figure 3A), suggesting that this phenotype is largely non-genetic.

The stochastic origin of the observed laterality defects is a striking finding, with potentially important conceptual consequences for our interpretation of variable disease phenotypes (see Discussion). However, the stochastic nature of the phenotype numbers makes it more difficult to identify the molecular origin of DFC number fluctuations. We therefore tried

to identify general principles that underlie DFC number variability. As both the DFCs and the surrounding dorsal domain are induced by high levels of Nodal in a non-cell-autonomous manner (Oteíza et al. 2008; Hagos and Dougan 2007), we reasoned that there could be a direct correlation between the number of cells forming the dorsal organizer and the DFCs number; however, we didn't find such an association (Figure S3A,B). Furthermore, we only found a weak association between maternal age and DHL frequency at 28.5ºC (Figure S3C).

Next, since DHL has been considered a spontaneous strain-dependent defect (Malicki et al. 2011), we compared the frequencies of reversed heart laterality between embryos with TL genetic background (the one used so far) versus AB. Interestingly, we found significantly lower DHL frequencies for AB embryos at 28.5ºC (1.3%, sd = 1.3%, IO = 22, n = 2714) and 33°C (7.7%, sd = 4.1%, IO = 34, n = 3353) compared to TL (Figure 3B). In line with this observation, we found that the number of DFCs and KV cells was higher in AB versus TL (Figure 3C), and that the antero-posterior cilia distribution is more asymmetric in AB than in TL (Figure S3D,E).

The strain-specific differences in DFC numbers gave us a handle to explore the molecular mechanism in more detail. Specifically, we hypothesized that the fluctuations might be maternally controlled, since DFCs begin to be emerge 1 hour after maternal-to-zygotic transition. To test this hypothesis, we crossed AB females with TL males and vice versa. Indeed, we found that the number of DFCs depends mostly on the mother's genetic background, as the cell numbers of the two hybrid crosses were different from each other (Figure 3D , with the TL (female) / AB (male) cross resembling the TL/TL cross, and the AB (female) / TL (male) cross resembling the AB/AB cross (Figure 3C,D). Consequently, a major source of the observed fluctuations in the embryo must lie in the development of the oocytes in the mother. When comparing TL and AB embryos by RNA-seq, we found 94 genes that were consistently differentially expressed in the period before and after the zygotic genome activation (2.25 hpf and 3.25 hpf, respectively) as well as the time window during which the DFCs are specified (4.25 - 5.25 hpf) (Figure 3E, Supplemental Figure 4, Table 1). 12 of the differentially expressed

genes are reported to have an early expression in specific cell types or structures (Figure 3F; ZFIN database of gene expression patterns). It is very likely that most of these differentially expressed genes are related to processes other than DFC specification that differ between the two strains. However, we were intrigued to find that 7 of these 12 genes with a reported early spatial pattern are expressed in cell types related to DFC specification – the enveloping layer (EVL), from which the DFCs are derived (Cooper and D'Amico 1996; Oteíza et al. 2008), and the yolk syncytial layer (YSL), which remains connected to the DFCs until 4hpf (Cooper and D'Amico 1996).

We found a high correlation in the expression levels of several of the differentially expressed YSL/EVL genes across the TL embryos (Figure 3G, Supplemental Figure 4). This raises the possibility that variation of some upstream factor (or a combination of factors) acting during oocyte development may be responsible for the observed variable but correlated expression. Interestingly, the mutant for one of these genes, *ctsba,* has been reported to have a reduced number of EVL cells (Langdon et al. 2016). However, it is unlikely that the genes identified here are the only ones responsible for variable DFC numbers, since additional factors (such as fluctuations in protein levels) may contribute equally. Furthermore, additional genes without a reported YSL/EVL expression might also be involved in this phenomenon. In summary, these experiments suggest that variable deposition of maternal factors, possibly involved in YSL/EVL specification and function, may be responsible for the observed fluctuations in DFC numbers.

Discussion

We found that stochastic fluctuations of a small cell population generated during the earliest stages of embryogenesis (the DFCs) are not corrected over the course of development, but instead persist and give rise to a macroscopic phenotype (defects of organ laterality). While it was reported before that left-right patterning in wildtype zebrafish is surprisingly variable (Noël

et al. 2013; Wang et al. 2011) and that there is a size threshold for reliable functioning of the KV (Sampaio et al. 2014; Gokey et al. 2015), we now show that these phenomena are linked and originate in fluctuations of DFC numbers that are at least partially caused by variable deposition of maternal factors.

Here we show that the number of cells in the KV is important for proper function. However, other studies have shown that the internal architecture is equally critical, since a higher density of cilia in the anterio-dorsal region is needed to create a proper leftward flow (Kreiling et al. 2007; Okabe, Xu, and Burdine 2008). We observed differences in cilia density ratio between AB and TL strains (Figure S3E), but no correlation to the cilia number (data not shown). If and how variation in DFC number is linked to morphological asymmetries in the KV is an interesting question, which would require additional live experiments.

The sizes of progenitor populations in vertebrate embryos are inherently variable due to environmental, genetic and stochastic fluctuations. Without feedback control, the size of the final cell population would dependent linearly on the size of the progenitor pool and hence be highly volatile (Lander et al. 2009). It is therefore remarkable that in this case there seem to be no corrective mechanisms that reduce cell number variability and thereby ensure robust left-right patterning. Furthermore, while mouse embryos pass a size checkpoint at around the time of gastrulation (Snow and Tam 1979; Lewis and Rossant 1982), the externally developing zebrafish embryos don't seem to pass such a checkpoint and are apparently evolved to maximize the speed of development, even at the cost of occasional laterality defects.

Here we investigated the consequences of developmental variability in a specific cell population, the DFCs, and it remains to be answered how general such phenomena are in other cell populations. How variable vertebrate development is, and which degree of fluctuations is still compatible with normal development, are important open questions, which will require novel experimental approaches such as high-throughput lineage tracing (Spanjaard et al. 2018; B. Raj et al. 2018; Alemany et al. 2018).

While stochastic developmental defects of this frequency and severity are probably not very common in wildtype mammals, it is likely that similar mechanisms as the one described here may underlie incomplete penetrance of mutations in model organisms (A. Raj et al. 2010; Burga, Casanueva, and Lehner 2011) as well as in humans. Furthermore, there is increasing evidence that disease phenotypes that manifest late in life, like Alzheimer's disease, may already originate in development (Arendt, Stieler, and Ueberham 2017). A similar phenomenon may occur in type I diabetes – an emerging view is that the initial pool of beta cells at the end of development is variable between individuals, leading to increased disease susceptibility in a subset of the population (Atkinson et al. 2015).We therefore speculate that early stochastic fluctuations of progenitor cell pools might at least partially contribute to a variety of human disease phenotypes.

Author contributions

J.P.J. and R.M.A. conceived and designed the project. R.M.A performed experiments and analyzed the data, with support by P.O.C. and R.S.. J.P.J. guided experiments and data analysis. All authors discussed and interpreted the results. R.M.A. and J.P.J. wrote the manuscript, with input from P.O.C..

Acknowledgements

We acknowledge support by the MDC/BIMSB core facilities for zebrafish and advanced light microscopy (especially Anca Margineanu), Jana Richter for help with animal experiments and Nancy Coconi-Linares for artwork. Work in J.P.J.'s laboratory was funded by a European Research Council Starting Grant (ERC-StG 715361 SPACEVAR). R.M.A. was supported by a CONACyT (Mexico) postdoctoral fellowship (CVU 269440).

Declaration of interests

The authors declare no competing interests.

284 **Figures**

285

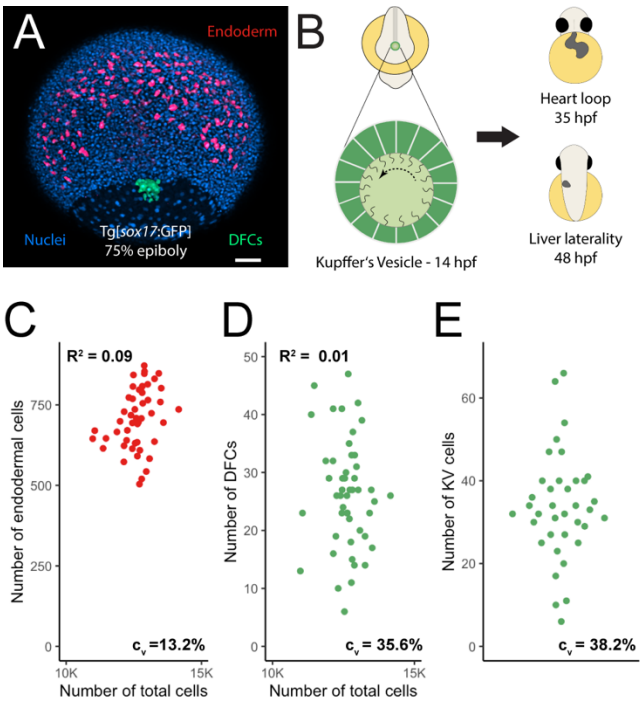

286

287 **Figure 1. Cell number variability during early embryogenesis.** (A) Maximum projection of
288 confocal images of a Tg[*sox17*:GFP] embryo at 75% epiboly stage showing the endoderm (red),
289 DFCs (green) and nuclei (blue). Scale bar = 80µm. (B) Graphical representation of and 8-somite
290 stage embryo and the KV (based on figures from Dasgupta et al. 2018), together with its role
291 in determining organ laterality. (C-E) Cell number in endoderm (n = 49), DFCs (n = 49) and
292 KV (n = 37) for individual embryos. The coefficient of variation (C_V) is indicated at the bottom
293 right, (C-D) also show the total cell number on the x-axis (C_V = 4.8%) and the coefficient of
294 determination (R^2).

295

296

297

298

299

300

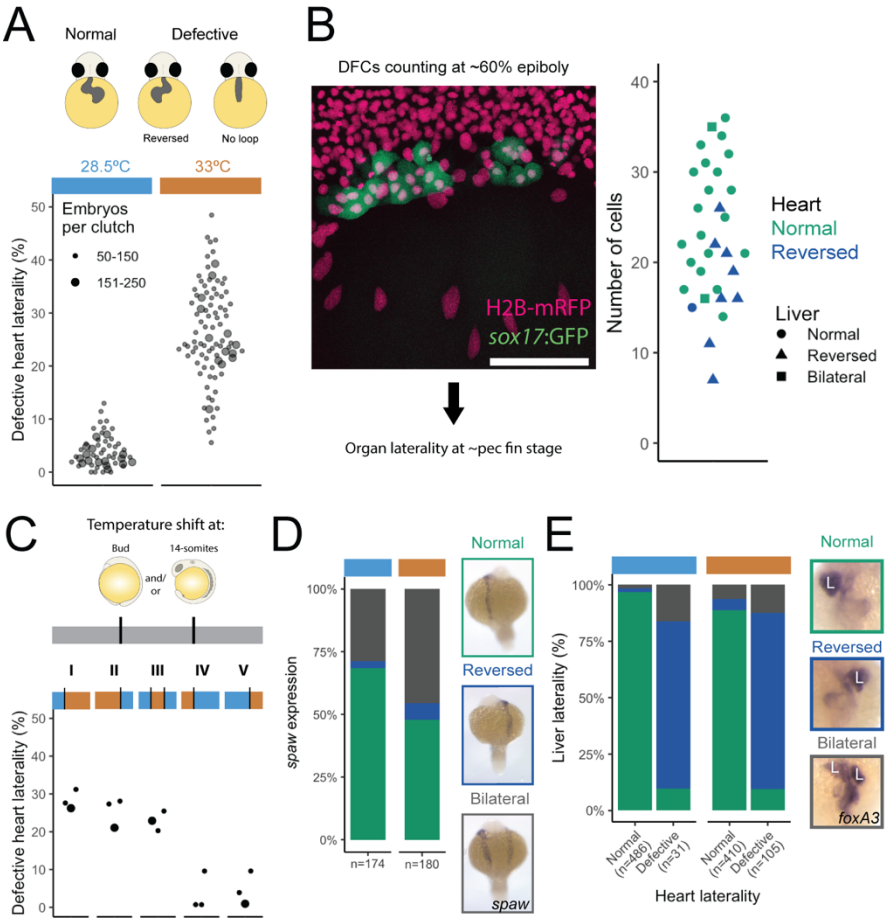

Figure 2. Fluctuations of DFC numbers lead to defects of organ laterality. (A) Heart laterality phenotypes scheme observed at prim-22 stage: normal (d-loop) and defective, which includes reversed (s-loop) and no heart loop, observed in embryos incubated at 28.5ºC (blue) and 33ºC (orange). The column scatter plots show the percentage of embryos with defective heart laterality per individual clutch analyzed at 28.5º (marked by the horizontal light blue bar) and 33ºC (orange bar). The small circles indicate a clutch size of 50-150 and the bigger ones a range of 151-250 embryos. (B) Confocal z-projection of the dorsal side of a Tg[*sox17*:GFP] (green) live embryo injected with H2B-mRFP (pink). The plot shows the DFC number distribution at 60% epiboly and the resulting heart and liver laterality in the individual embryos assessed by *in situ* hybridization (n = 31). (C) Graphical representation of the different temperature shift treatments: the first third of the gray bar represents the period between 1-cell and bud stage, the second until the 14-somite stage, and the third until the period of collection (long pec stage). Circle size as in (A). Bud and 14-somite schemes are based on Kimmel et al.

1995. (D) Relative frequency of different *spaw* expression patterns in embryos incubated at 28.5º and 33ºC. *in situ* hybridization photographs of normal (green), reversed (dark blue) and bilateral (gray) *spaw* expression in 18-somite stage embryos are shown to the right. (E) Relative frequency of embryos with normal, reversed or bilateral liver, separated into embryos with normal or defective heart laterality (incubated at 28.5º or 33ºC). To the right: Liver laterality as measured by *foxA3 in situ* hybridization.

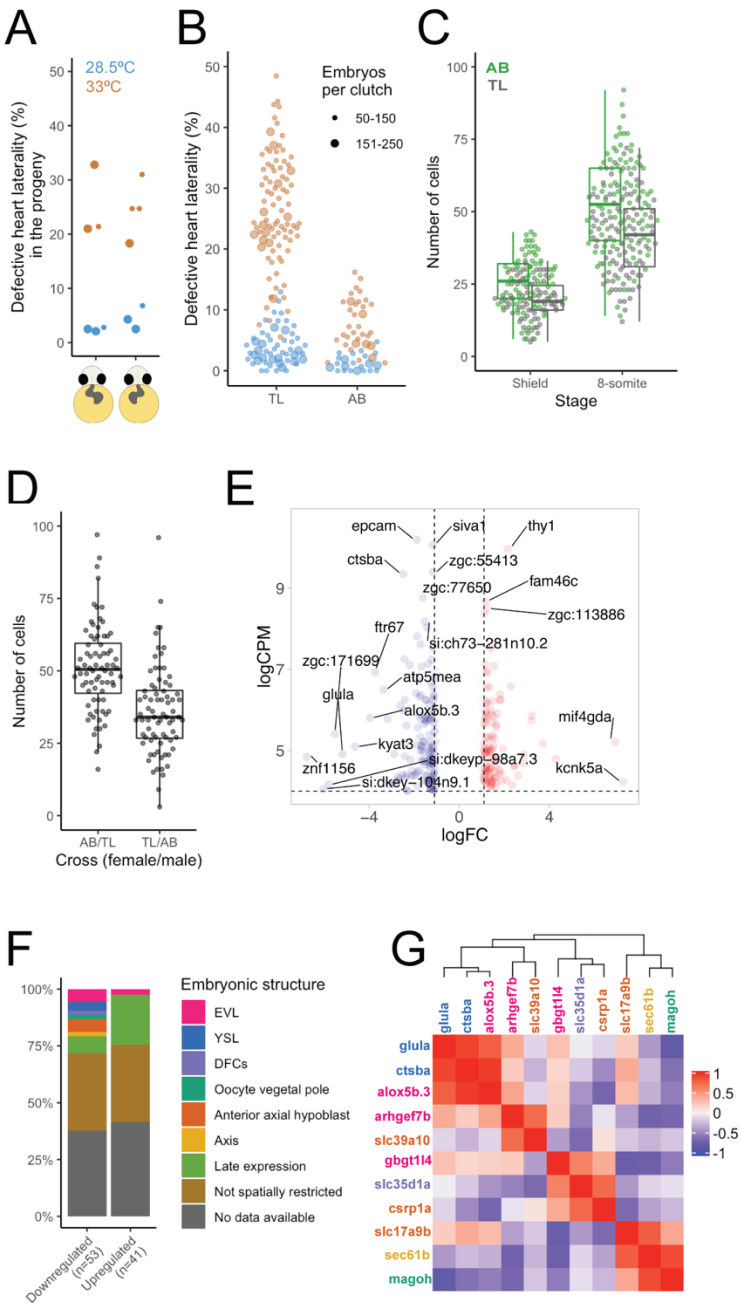

Figure 3. Heart laterality defects are a stochastic phenomenon that is linked to variable deposition of maternal factors. (A) Percentage of embryos with defective heart laterality in the progeny of individuals that showed either normal or reversed heart laterality at prim-22 stage. Incubation temperature 28.5ºC (light blue) or 33ºC (orange). The small points indicate a clutch size ranging of 50-150 and the bigger points for a range of 151-250. (B) Percentage of embryos with defective heart laterality per individual clutch analyzed at 28.5º and 33ºC in TL (same data as Figure 2A) and AB embryos. (C) Number of DFCs / KV cells at shield and 8-

somite stage; for shield stage: n = 78 and 75 for AB and TL, respectively, $p < 0.001$; for 8-somite stage: n = 94 and 97 AB and TL, respectively, $p < 0.001$). (D) KV cell numbers at 8-somite stage in crosses between individual AB and TL males and females, AB/TL vs TL/AB $p < 0.001$ (n=76 for both); AB vs AB/TL $p = 0.461$; TL vs TL/AB $p = 0.01$; AB vs TL/AB $p < 0.001$; TL vs AB/TL $p < 0.001$. (E) Volcano plot ($\log_2$ of the counts per million (CPM) and fold change (FC)) showing differentially expressed genes in TL compared to AB embryos at 2.25 hpf determined by RNA-seq. The top 20 DE genes are shown. (F) Summary of reported embryonic expression patterns for the down- and upregulated genes. (G) Pairwise Pearson correlation between the downregulated genes at 2.25hpf for TL embryos. The gene names are color-coded by embryonic structure as in (F). Color scale to the right. The boxplots in (C) and (D) display the median; the hinges represent the first and third quartiles and the whiskers represent 1.5 of the inter-quartile range from the hinge.

Methods

Zebrafish Husbandry and Staging

All animal procedures were conducted according to local authorities guidance (LAGeSo, Berlin, Germany). Adult zebrafish were maintained and bred under standard conditions. Embryos were left to develop in egg water (0.6 g/L dissolved in dH2O; Red Sea Salt, Red Sea, containing methylene blue, 0.002 g/L) to the desired stage at 28.5C unless otherwise stated. Staging was done based on Kimmel et al. 1995. It was not possible to record the sex of the embryos examined due to their developmental stage.

Zebrafish strains

AB and Tüpfel Long Fin (TL) strains were obtained from the European Zebrafish Research Center (EZRC). The Tg[*sox17*:GFP] strain was reported in (Sakaguchi et al. 2006). To change its genetic background to TL, the fish were crossed with TL fish. By crossing the resulting males with TL females, we obtained similar DHL percentages as in the TL wildtype strain.

Immunolocalization

Embryos at the desired stage were fixed overnight at 4ºC in PFA 4% in PBS. The following day, they were washed 3x with PBSTx (1x PBS with TritonX 1%) for 5 minutes and dechorionated. They were incubated in blocking buffer (2% BSA, 5% Goat Serum in PBSTx) for 2 hours at room temperature (RT), followed by an overnight incubation at 4ºC with one or a combination of the following primary antibodies diluted in blocking buffer: mouse anti-acetylated Tubulin (1:200, Sigma Aldrich T6793), chicken or rabbit anti-GFP (1:1000, Abcam ab13970 and ab290, respectively), rabbit anti-Flh (1:200, Sigma Aldrich SAB2702443) and rabbit anti-Laminin-α1β1γ1 (1:100, Sigma Aldrich L9393). On the next day, they were washed

3x with PBSTx and 1x with blocking buffer, 30 minutes each at RT, followed by an overnight incubation at 4ºC with Hoechst 1:1000 and secondary antibody diluted in blocking buffer (1:200): goat anti-chicken Alexa-488 (Thermo Fisher A11039), goat anti-mouse Alexa-647 (Thermo Fisher A32728) or goat anti-rabbit Alexa-568 (Thermo Fisher A11011). Finally, 3x PBSTx washes, 30 minutes each at RT.

Imaging

Endodermal, DFCs and total cell number in 75% epiboly embryos: after anti-GFP immunolocalization, the embryos were washed with 50% glycerol/50% PBSTx for ten minutes and then with 100% glycerol overnight at 4ºC. For flat mount, a layer of laboratory labeling tape (13mm wide) was attached to each side of a coverslip to make a bridge and leave enough room for the flat embryo (~120µm). A single embryo was put on a coverslip with a drop of glycerol. For flattening, a closed forceps was introduced in the vegetal pole and then opened to break and split the yolk cell in half. As many yolk granules as possible were removed to avoid damaging the blastoderm, then another coverslip was put on top. The tissue was oriented facing the bottom to be imaged with an SP8 inverted confocal microscope. After obtaining an image stack for the endodermal and total cell number, another stack was obtained for the DFCs region with lower laser power and higher zoom factor, since the GFP signal intensity in these cells is considerably higher than in the endodermal cells. SP8 microscope acquisition parameters: 20x multi-immersion objective, format = 1024 x 1024, speed = 600, zoom factor = 0.75 (except for DFCs, 2 or 4 when all cells fit), line average = 2, Z-step size = 3, gating = 0.3 - 6 for both channels, laser intensity Z-compensation for each image, tiling = 2x2 in most images, with 15% overlapping. The images were automatically stitched with the Leica software.

For imaging DFCs at shield, cilia at 8-somite stage and total amount of cells at different stages (3.25-5.25hpf), the embryos were mounted in 1% low melting point agarose, and imaged on an upright Zeiss 880 confocal microscope, with the following settings: 20x water-dipping

objective, format = 512 x 512, speed = 8, zoom factor = 1, line average = 2, Z-step size = 3. For the total amount of cell counting a 2-photon Chameleon laser was used, tiling = 2x2, with 15% overlapping. The images were automatically stitched with the Zeiss software.

Live imaging

For KV measurements at 8-somite stage, embryos incubated at 28.5º or 33ºC were mounted on a 1.5% agarose injection dish with little liquid. The embryos were oriented inside the chorion to image the KV. Afterwards, 3% methylcellulose in E3 embryo medium (5mM NaCl, 0.17mM KCl, 0.33mM $CaCl_2$, 0.33mM $MgSO_4$) was added to cover the embryos and, thus, retain the order of the individual embryos. The embryos were incubated at the initial temperature until prim-22 for heart laterality analysis. Per session, around 30 embryos were imaged for each condition.

For DFC counting, individual Tg[*sox17*:GFP] (injected with ~60 pg of H2B-mRFP mRFP1 at one-cell stage) shield stage embryos were transferred to glass-bottom Petri dishes, most of the liquid was removed and ~0.5 mL of 3% methylcellulose in E3 embryo medium was added. Then, the embryos were manually dechorionated with forceps and oriented with the shield facing the bottom of the dish for imaging on the Leica SP8 confocal microscope. After imaging, the dish was filled with E3 embryo medium and incubated at 33ºC until long pec stage and fixed for *in situ* hybridization.

***in situ* hybridization**

Whole-mount in situ hybridizations were performed essentially as described previously (Thisse & Thisse, 2008). The following probes were used: *sox32* (Bjornson et al. 2005); *foxA3* and *myl7* (Noël et al. 2013); and *spaw* and *dand5* (Sampaio et al. 2014).The *amhc* probe was kindly provided by Daniela Panáková.

453 **mRNA synthesis**

454 The H2B-mRFP1 mRNA was synthesized using the mMESSAGE mMACHINE kit
455 (Thermo Fisher AM1345) according to the manufacturer's recommendations.

456

457 **Temperature shift treatment**

458 After collection, the embryos were put immediately in warmed water, either to 28.5ºC
459 or 33ºC. For the temperature shift, the embryos were transferred to a Petri dish filled with water
460 at the desired temperature.

461

462 **Single embryo RNA-seq**

463 A total of 6 AB and 6 TL embryos were individually collected per stage (2.25, 3.25,
464 4.25 and 5.25 hpf) in LoBind tubes (Eppendorf) in two independent experiments (each of which
465 contained half of the samples for each condition). 0.5mL Trizol and 0.5µl GlycoBlue were
466 added to each samples, and RNA extraction was carried according to the manufacturer's
467 recommendations. Each sample was barcoded, pooled and the libraries were prepared according
468 to the CEL-seq2 protocol (Hashimshony et al. 2016) with different RPI indices for each
469 timepoint and paired-end sequenced on an Illumina NextSeq 500 (read length 12 nt for barcode
470 read and 63 nt for transcript read).

471

472 **Sequencing data analysis**

473 Basecalling was done with bcl2fastq v2.19.0.316. The resulting reads were
474 demultiplexed with *scruff* (Wang et al. 2019). Mapping was done with STAR 2.7.1a (Dobin et
475 al. 2013) using quantMode GeneCounts and the DanRer11v96 transcriptome as reference.
476 Differentially expressed (DE) genes were obtained with edgeR (Robinson, McCarthy, and
477 Smyth 2009). Genes with a False Discovery Rate < 0.01, log Counts Per Million > 4 and log
478 Fold Change < -1 for downregulated and > 1 for upregulated genes were considered DE. Spatial

and temporal expression was obtained on The Zebrafish Information Network (Bradford et al. 2011).

Plots

All plots were generated in R using the following additional libraries: ggplot2 graphing package, ggbeswarm for column scatter plots, ggExtra for marginal histograms and ComplexHeatMap for heatmaps; for which, a logarithmic transformation of the counts per million (CPM) values obtained with edgeR was applied first. Volcano plots were generated with VolcaNoseR (Goedhart and Luijsterburg 2020).

Cell counting

The endodermal cells were counted with the Imaris (Bitplane) Surface module: background subtraction: on, diameter of largest sphere: 15 µm, splicing touching: on, seed points diameter: 8 µm. For each sample, the number was visually corroborated. The total cell number was estimated with the Fiji (Schindelin et al. 2012) ITCN plugin. A Z-projection was obtained for each stack, the ITCN parameters were: width 12, minimum distance 6, threshold: 0.5.

For quantification of dorsal domain cells and DFCs, cell number was estimated manually for cilia with the Cell Counter Fiji plugin. The cilia number was used as a proxy for the KV cell number, since the cells are monociliated. DFCs numbers were first estimated with ITCN (width 18, minimum distance 9, threshold: 0.5) and visually corrected afterwards. For the total amount of cell estimation, the cells were counted with Imaris, same parameters mentioned above.

The Flh positive cells were counted with ITCN plugin (same parameters used for DFCs mention above). In all cases the embryos were imaged immediately after immunolocalization. The

number of dorsal domain cells was obtained by subtracting the DFCs number from the number of Flh positive cells, since Flh is also expressed in the DFCs.

Statistics

The coefficients of determination were obtained with R. The p-values are obtained with a randomization test done with PlotsOfDifferences (Goedhart 2019). All statistical parameters, including samples numbers and median are shown in the figures, described in the figure legends or in the main text.

Supplemental files

Video 1. Heart loop phenotypes observed at prim-22 stage. Heart laterality phenotypes on live embryos; normal/dextral loop (d-loop); defective includes: reversed/sinistral loop (s-loop) and no loop, shown side by side on a ventral view.

Table 1. Shared DE genes. Function, earliest expression, spatial expression, DE expression, and embryonic structure information from ZFIN for the differentially expressed genes found across the timepoints selected for AB vs TL comparison.

555 **References**

556

557 Alemany, Anna, Maria Florescu, Chloé S. Baron, Josi Peterson-Maduro, and Alexander Van
558 Oudenaarden. 2018. "Whole-Organism Clone Tracing Using Single-Cell Sequencing."
559 *Nature* 556 (7699): 108–12. https://doi.org/10.1038/nature25969.
560 Alexander, J, M Rothenberg, G L Henry, and D Y Stainier. 1999. "Casanova Plays an Early
561 and Essential Role in Endoderm Formation in Zebrafish." *Developmental Biology* 215:
562 343–57. https://doi.org/10.1006/dbio.1999.9441.
563 Amack, Jeffrey D., and HJ. Yost. 2004. "The T Box Transcription Factor No Tail in Ciliated
564 Cells Controls Zebrafish Left-Right Asymmetry." *Current Biology* 128 (2): 189–90.
565 https://doi.org/10.1016/j.
566 Arendt, Thomas, Jens Stieler, and Uwe Ueberham. 2017. "Is Sporadic Alzheimer′s Disease a
567 Developmental Disorder?" *Journal of Neurochemistry* 143 (4): 396–408.
568 https://doi.org/10.1111/jnc.14036.
569 Atkinson, Mark, Matthias von Herrath, Alvin C Powers, and Michael Clare-Salzler. 2015.
570 "Current Concepts on the Pathogenesis of Type 1 Diabetes d Considerations for
571 Attempts to Prevent and Reverse the Disease." *Diabetes Care* 38 (June): 979–88.
572 https://doi.org/10.2337/dc15-0144.
573 Barkai, Naama, and Ben Zion Shilo. 2009. "Robust Generation and Decoding of Morphogen
574 Gradients." *Cold Spring Harbor Perspectives in Biology* 1 (5): 1–15.
575 https://doi.org/10.1101/cshperspect.a001990.
576 Bjornson, Christopher R R, Kevin J P Griffin, Gist H. Farr, Akira Terashima, Charis Himeda,
577 Yutaka Kikuchi, and David Kimelman. 2005. "Eomesodermin Is a Localized Maternal
578 Determinant Required for Endoderm Induction in Zebrafish." *Developmental Cell* 9 (4):
579 523–33. https://doi.org/10.1016/j.devcel.2005.08.010.
580 Bradford, Yvonne, Tom Conlin, Nathan Dunn, David Fashena, Ken Frazer, Douglas G.

581 Howe, Jonathan Knight, et al. 2011. "ZFIN: Enhancements and Updates to the Zebrafish
582 Model Organism Database." *Nucleic Acids Research* 39 (SUPPL. 1): 822–29.
583 https://doi.org/10.1093/nar/gkq1077.
584 Briscoe, James, and Stephen Small. 2015. "Morphogen Rules: Design Principles of Gradient-
585 Mediated Embryo Patterning." *Development* 142 (23): 3996–4009.
586 https://doi.org/10.1242/dev.129452.
587 Burga, Alejandro, M. Olivia Casanueva, and Ben Lehner. 2011. "Predicting Mutation
588 Outcome from Early Stochastic Variation in Genetic Interaction Partners." *Nature* 480
589 (7376): 250–53. https://doi.org/10.1038/nature10665.
590 Cooper, M S, and L a D'Amico. 1996. "A Cluster of Noninvoluting Endocytic Cells at the
591 Margin of the Zebrafish Blastoderm Marks the Site of Embryonic Shield Formation."
592 *Developmental Biology* 180 (0294): 184–98. https://doi.org/10.1006/dbio.1996.0294.
593 Dasgupta, Agnik, Matthias Merkel, Madeline J Clark, Andrew E Jacob, Jonathan Edward
594 Dawson, M Lisa Manning, and Jeffrey D Amack. 2018. "Cell Volume Changes
595 Contribute to Epithelial Morphogenesis in Zebrafish Kupffer's Vesicle." *ELife* 7: 1–34.
596 https://doi.org/10.7554/eLife.30963.
597 Dobin, Alexander, Carrie A. Davis, Felix Schlesinger, Jorg Drenkow, Chris Zaleski, Sonali
598 Jha, Philippe Batut, Mark Chaisson, and Thomas R. Gingeras. 2013. "STAR: Ultrafast
599 Universal RNA-Seq Aligner." *Bioinformatics* 29 (1): 15–21.
600 https://doi.org/10.1093/bioinformatics/bts635.
601 El-Brolosy, Mohamed A., Zacharias Kontarakis, Andrea Rossi, Carsten Kuenne, Stefan
602 Günther, Nana Fukuda, Khrievono Kikhi, et al. 2019. "Genetic Compensation Triggered
603 by Mutant MRNA Degradation." *Nature* 568 (7751): 193–97.
604 https://doi.org/10.1038/s41586-019-1064-z.
605 Essner, Jeffrey J, Jeffrey D Amack, Molly K Nyholm, Erin B Harris, and H Joseph Yost.
606 2005. "Kupffer's Vesicle Is a Ciliated Organ of Asymmetry in the Zebrafish Embryo

That Initiates Left-Right Development of the Brain, Heart and Gut." *Development* 132 (6): 1247–60. https://doi.org/10.1242/dev.01663.

Gaspar, Pedro, Saad Arif, Lauren Sumner-rooney, Maike Kittelmann, Andrew J Bodey, David L Stern, Maria D S Nunes, and Alistair P Mcgregor. 2020. "Characterization of the Genetic Architecture Underlying Eye Size Variation Within Drosophila Melanogaster and Drosophila Simulans." *G3* 10 (March): 1005–18.

Goedhart, Joachim. 2019. "PlotsOfDifferences - a Web App for the Quantitative Comparison of Unpaired Data." *BioRxiv*. https://doi.org/10.1101/578575.

Goedhart, Joachim, and Martijn S Luijsterburg. 2020. "VolcaNoseR – a Web App for Creating , Exploring and Sharing Volcano Plots." *BioRxiv*. https://doi.org/10.1101/2020.05.07.082263 .

Gokey, Jason J., Agnik Dasgupta, and Jeffrey D. Amack. 2015. "The V-ATPase Accessory Protein Atp6ap1b Mediates Dorsal Forerunner Cell Proliferation and Left-Right Asymmetry in Zebrafish." *Developmental Biology* 407 (1): 115–30. https://doi.org/10.1016/j.ydbio.2015.08.002.

Gokey, Jason J., Yongchang Ji, Hwee Goon Tay, Bridget Litts, and Jeffrey D. Amack. 2015. "Kupffer's Vesicle Size Threshold for Robust Left-Right Patterning of the Zebrafish Embryo." *Developmental Dynamics*, 22–33. https://doi.org/10.1002/dvdy.24355.

Hagos, Engda G, and Scott T Dougan. 2007. "Time-Dependent Patterning of the Mesoderm and Endoderm by Nodal Signals in Zebrafish." *BMC Developmental Biology* 18: 1–18. https://doi.org/10.1186/1471-213X-7-22.

Hashimoto, Hisashi, Michael Rebagliati, Nadira Ahmad, Osamu Muraoka, Tadahide Kurokawa, Masahiko Hibi, and Tohru Suzuki. 2004. "The Cerberus/Dan-Family Protein Charon Is a Negative Regulator of Nodal Signaling during Left-Right Patterning in Zebrafish." *Development* 131 (8): 1741–53. https://doi.org/10.1242/dev.01070.

Hashimshony, Tamar, Naftalie Senderovich, Gal Avital, Agnes Klochendler, Yaron de

633 Leeuw, Leon Anavy, Dave Gennert, et al. 2016. “CEL-Seq2: Sensitive Highly-
634 Multiplexed Single-Cell RNA-Seq.” *Genome Biology* 17 (1): 1–7.
635 https://doi.org/10.1186/s13059-016-0938-8.
636 Hunt, Edmund R, Ciara Dornan, Ana B Sendova-franks, and Nigel R Franks. 2018.
637 “Asymmetric Ommatidia Count and Behavioural Lateralization in the Ant Temnothorax
638 Albipennis.” *Scientific Reports*, 1–11. https://doi.org/10.1038/s41598-018-23652-4.
639 Imai, Y, M a Gates, a E Melby, D Kimelman, a F Schier, and W S Talbot. 2001. “The
640 Homeobox Genes Vox and Vent Are Redundant Repressors of Dorsal Fates in
641 Zebrafish.” *Development* 128 (12): 2407–20.
642 http://www.ncbi.nlm.nih.gov/pubmed/11493559.
643 Kimmel, Charles B., William Ballard, Seth R Kimmel, Bonnie Ullman, and Thomas F.
644 Schilling. 1995. “Stages of Embryonic Development of the Zebrafish.” *Developmental*
645 *Dynamics* 203: 255–310.
646 Kreiling, Jill A., Prabhat, Geoffrey Williams, and Robbert Creton. 2007. “Analysis of
647 Kupffer’s Vesicle in Zebrafish Embryos Using a Cave Automated Virtual Environment.”
648 *Developmental Dynamics* 236 (7): 1963–69. https://doi.org/10.1002/dvdy.21191.
649 Lander, Arthur D, Kimberly K Gokoffski, Frederic Y M Wan, Qing Nie, and Anne L Calof.
650 2009. “Cell Lineages and the Logic of Proliferative Control” 7 (1).
651 https://doi.org/10.1371/journal.pbio.1000015.
652 Langdon, Yvette G., Ricardo Fuentes, Hong Zhang, Elliott W. Abrams, Florence L. Marlow,
653 and Mary C. Mullins. 2016. “Split Top: A Maternal Cathepsin B That Regulates
654 Dorsoventral Patterning and Morphogenesis.” *Development* 143 (6): 1016–28.
655 https://doi.org/10.1242/dev.128900.
656 Lewis, N. E., and J. Rossant. 1982. “Mechanism of Size Regulation in Mouse Embryo
657 Aggregates.” *Journal of Embryology and Experimental Morphology* Vol. 72 (1): 169–
658 81.

659 Malicki, Jarema, Andrei Avanesov, Jade Li, Shiaulou Yuan, and Zhaoxia Sun. 2011. *Analysis*
660 *of Cilia Structure and Function in Zebrafish*. *Methods in Cell Biology*. Third Edit. Vol.
661 101. Elsevier Ltd. https://doi.org/10.1016/B978-0-12-387036-0.00003-7.
662 Megason, Sean G. 2009. *In Toto Imaging of Embryogenesis with Confocal Time-Lapse*
663 *Microscopy. Mol Biol.* Vol. 546. https://doi.org/10.1007/978-1-62703-239-1_1.
664 Melby, a E, R M Warga, and C B Kimmel. 1996. "Specification of Cell Fates at the Dorsal
665 Margin of the Zebrafish Gastrula." *Development* 122: 2225–37.
666 Noël, Emily S, Manon Verhoeven, Anne Karine Lagendijk, Federico Tessadori, Kelly Smith,
667 Suma Choorapoikayil, Jeroen den Hertog, and Jeroen Bakkers. 2013. "A Nodal-
668 Independent and Tissue-Intrinsic Mechanism Controls Heart-Looping Chirality." *Nature*
669 *Communications* 4 (August 2015): 2754. https://doi.org/10.1038/ncomms3754.
670 Okabe, Noriko, Bo Xu, and Rebecca D. Burdine. 2008. "Fluid Dynamics in Zebrafish
671 Kupffer's Vesicle." *Developmental Dynamics* 237 (12): 3602–12.
672 https://doi.org/10.1002/dvdy.21730.
673 Oteíza, Pablo, Mathias Köppen, Miguel L Concha, and Carl-Philipp Heisenberg. 2008.
674 "Origin and Shaping of the Laterality Organ in Zebrafish." *Development* 135 (16): 2807–
675 13. https://doi.org/10.1242/dev.022228.
676 Raj, Arjun, Scott a Rifkin, Erik Andersen, and Alexander van Oudenaarden. 2010.
677 "Variability in Gene Expression Underlies Incomplete Penetrance." *Nature* 463 (7283):
678 913–18. https://doi.org/10.1038/nature08781.
679 Raj, Bushra, Daniel E. Wagner, Aaron McKenna, Shristi Pandey, Allon M. Klein, Jay
680 Shendure, James A. Gagnon, and Alexander F. Schier. 2018. "Simultaneous Single-Cell
681 Profiling of Lineages and Cell Types in the Vertebrate Brain." *Nature Biotechnology* 36
682 (5): 442–50. https://doi.org/10.1038/nbt.4103.
683 Ramaekers, Ariane, Annelies Claeys, Martin Kapun, Emmanuèle Mouchel-Vielh, Delphine
684 Potier, Simon Weinberger, Nicola Grillenzoni, et al. 2019. "Altering the Temporal

685 Regulation of One Transcription Factor Drives Evolutionary Trade-Offs between Head
686 Sensory Organs Article Altering the Temporal Regulation of One Transcription Factor
687 Drives Evolutionary Trade-Offs between Head Sensory Organs." *Developmental Cell*
688 50: 780–92. https://doi.org/10.1016/j.devcel.2019.07.027.
689 Robinson, Mark D., Davis J. McCarthy, and Gordon K. Smyth. 2009. "EdgeR: A
690 Bioconductor Package for Differential Expression Analysis of Digital Gene Expression
691 Data." *Bioinformatics* 26 (1): 139–40. https://doi.org/10.1093/bioinformatics/btp616.
692 Sakaguchi, Takuya, Yutaka Kikuchi, Atsushi Kuroiwa, Hiroyuki Takeda, and Didier Y R
693 Stainier. 2006. "The Yolk Syncytial Layer Regulates Myocardial Migration by
694 Influencing Extracellular Matrix Assembly in Zebrafish." *Development* 133 (20): 4063–
695 72. https://doi.org/10.1242/dev.02581.
696 Sampaio, Pedro, Rita R. Ferreira, Adán Guerrero, Petra Pintado, Bárbara Tavares, Joana
697 Amaro, Andrew A. Smith, Thomas Montenegro-Johnson, David J. Smith, and Susana S.
698 Lopes. 2014. "Left-Right Organizer Flow Dynamics: How Much Cilia Activity Reliably
699 Yields Laterality?" *Developmental Cell* 29 (6): 716–28.
700 https://doi.org/10.1016/j.devcel.2014.04.030.
701 Schindelin, Johannes, Ignacio Arganda-Carreras, Erwin Frise, Verena Kaynig, Mark Longair,
702 Tobias Pietzsch, Stephan Preibisch, et al. 2012. "Fiji: An Open-Source Platform for
703 Biological-Image Analysis." *Nature Methods* 9 (7): 676–82.
704 https://doi.org/10.1038/nmeth.2019.
705 Shah, Gopi, Konstantin Thierbach, Benjamin Schmid, Johannes Waschke, Anna Reade,
706 Mario Hlawitschka, Ingo Roeder, Nico Scherf, and Jan Huisken. 2019. "Multi-Scale
707 Imaging and Analysis Identify Pan-Embryo Cell Dynamics of Germlayer Formation in
708 Zebrafish." *Nature Communications* 10 (1): 5753. https://doi.org/10.1038/s41467-019-
709 13625-0.
710 Snow, M.H.L., and P.P.L Tam. 1979. "Is Compensatory Growth a Complicating Factor in

711 Mouse Teratology?" *Nature* 279 (9): 555–57.
712 https://doi.org/10.1017/CBO9781107415324.004.
713 Spanjaard, Bastiaan, Bo Hu, Nina Mitic, Pedro Olivares-Chauvet, Sharan Janjuha, Nikolay
714 Ninov, and Jan Philipp Junker. 2018. "Simultaneous Lineage Tracing and Cell-Type
715 Identification Using CRISPR–Cas9-Induced Genetic Scars." *Nature Biotechnology*
716 *2018*, no. April. https://doi.org/10.1038/nbt.4124.
717 Thisse, Christine, and Bernard Thisse. 2008. "High-Resolution in Situ Hybridization to
718 Whole-Mount Zebrafish Embryos." *Nature Protocols* 3 (1): 59–69.
719 https://doi.org/10.1038/nprot.2007.514.
720 Wang, Guangliang, Adam B Cadwallader, Duck Soo Jang, Michael Tsang, H Joseph Yost,
721 and Jeffrey D Amack. 2011. "The Rho Kinase Rock2b Establishes Anteroposterior
722 Asymmetry of the Ciliated Kupffer's Vesicle in Zebrafish." *Development* 138 (1): 45–
723 54. https://doi.org/10.1242/dev.052985.
724 Wang, Zhe, Junming Hu, W. Evan Johnson, and Joshua D. Campbell. 2019. "Scruff: An
725 R/Bioconductor Package for Preprocessing Single-Cell RNA-Sequencing Data." *BMC*
726 *Bioinformatics* 20 (1): 1–9. https://doi.org/10.1186/s12859-019-2797-2.
727 Warga, R M, and C Nüsslein-Volhard. 1999. "Origin and Development of the Zebrafish
728 Endoderm." *Development* 126 (4): 827–38.
729 Warga, Rachel M., and Donald A. Kane. 2018. "Wilson Cell Origin for Kupffer's Vesicle in
730 the Zebrafish." *Developmental Dynamics* 247 (9): 1057–69.
731 https://doi.org/10.1002/dvdy.24657.
732